

## Alternative-Current Electrochemical Etching of Uniform Porous Silicon for Photodetector Applications

Husnen R. Abd<sup>1</sup>, Y. Al-Douri<sup>1,\*</sup>, Naser M. Ahmed<sup>2</sup>, U. Hashim<sup>1</sup>

<sup>1</sup>Institute of Nano Electronic Engineering, University Malaysia Perlis, 01000 Kangar, Perlis, Malaysia

<sup>2</sup>School of Physics, University Sains Malaysia, 11800 Penang, Malaysia

\*E-mail: [yaldouri@yahoo.com](mailto:yaldouri@yahoo.com)

Received: 9 March 2013 / Accepted: 10 April 2013 / Published: 20 August 2013

---

The twining of alternative-current (AC) with electrochemical etching (ECE) to fabricate porous silicon (PS) is studied. The porosity percentage is obtained by gravimetric analysis. The effect of different current densities; 20, 25 and 30 mA/cm<sup>2</sup> at 30 min on morphology and electrical properties of PS have been investigated. The electrical properties of I-V characteristics, Schottky barrier height, photoresponse and responsivity of PS are analyzed. The quantum efficiency is measured under different current densities. The obtained results showed quite distinguished results for best performance of photodetectors.

---

**Keywords:** Porous silicon; Alternative current; Electrical properties.

### 1. INTRODUCTION

Crystalline silicon is most widely used in the integrated circuits industry. The anodic attack of single-crystal silicon has led to a wide range of mechanical sensor. In fact, under electrochemical etching of doped silicon wafer in (HF/Ethanol) solution, the metal on the back of doped Si wafer for using as ohmic contact and controlled current density leads to fabricate macro or nano porous silicon (PS) layers achieved by the standard direct current (DC) and alternating current (AC). PS has been widely used to achieve many interesting characteristics such as direct energy band gap [1]. Although microporous silicon presents a very high specific surface [2], PS may has optical properties completely different from the bulk but it retains the crystallinity of the substrate.

El-Bahar and Nemirovsky [3] have reported the formation of PS under alternating current (AC) conditions instead of applying direct current (DC) electrochemical process. They have explored the main advantages of (a) The alternating current formed PS and exhibit higher mechanical stability, (b)

The alternating current process can be performed without deposited backside contact. They have simplified the process, permitted its integration with high temperature processing steps and clean furnaces of a modern very large scale-integrated technology. Otherside, Barodovoi et al. [4] have studied the dark and light I-V characteristics as well as spectral curves of planar Ni-porous silicon-p-Si-Ni heterostructures. They have shown that the photogeneration in heterostructure occurs both in the region of thin PS layer and p-Si base. Avalanche breakdown is observed in the heterostructure at applied voltage biases  $V > 8-10$  V and  $T=77$  K. The coefficient of multiplying at  $V=11$  V that has been achieved at 60 (dark) and 200 (light) belongs to silicon  $n^+ - p-i-p^+$  avalanche photodiodes. While, Naderi and Hashim [5] have researched a combination of electroless and electrochemical etching of silicon surface for enhancing the uniformity of fabricated PS substrate and improving the sensitivity of photodetectors. They have modified photo-assisted pulsed electrochemical etching of silicon by introducing a novel parameter called delay time ( $T_d$ ), along with cycle time and pause time, of pulsed current, which can affect the morphology of pores. This technique offers the possibility of growing photoluminescent materials with uniform pores and selective wavelength emission. They have proved that within 2 min, a significant increasing of intensity of Raman spectrum is due to enhanced surface-assisted multi-phonon processes in porous film. A redshift of  $2.5 \text{ cm}^{-1}$  and a peak broadening of 1.4 times has been observed for this porous sample compared with those of crystalline silicon. And theoretically, Al-Douri et al. [6] have achieved theoretical works about using empirical pseudopotential method (EPM) to calculate the energy gap of Si which is found to be indirect. They have investigated features such as refractive index, optical dielectric constant, bulk modulus, elastic constants and short- range force constants have. Also, they have derived the shear modulus, Young's modulus, Poisson's ratio and Lamé's constants for both bulk Si and PS. They found that the Debye temperature of PS is estimated from the average sound velocity.

In this work, we have fabricated PS using photoelectrochemical etching (PECE) with alternating current (AC) and have prepared Schottky devices by choosing n-type (100) at different current densities with constant etching time. The morphology of PS is studied. I-V characteristics under forward bias Schottky barrier heights, ideality factor at room temperature, photoresponse and responsivity are measured for photodetectors applications.

## 2. EXPERIMENTAL PROCESS

Single crystal wafer of n-type (100) Si of 1-10  $\Omega \cdot \text{cm}$  resistance were cut into square with area  $1.7 \text{ cm}^2$ . The silicon wafer was cleaned by Radio Corporation of America method (RCA) before PS formation. For PS fabrication, we have used anodization cell which is made from Teflon. The silicon wafer fixed and sealed through O-ring, the front side of the silicon wafer is contacted with the solution (HF: ethanol) and the back side is contact with the copper to get contact. Figure 1 shows the set-up of PS formation.

The Si wafer was immersed by a mixture of electrolyte solution HF, 48% and ethanol, 98% concentrations. The aim of this addition is helping to remove the  $\text{H}_2$  gas bubbles from the sample

surface that formed during the anodization process [7], the Si wafer acts as the anode and the cathode is made of platinum or other HF-resistant conductive material.

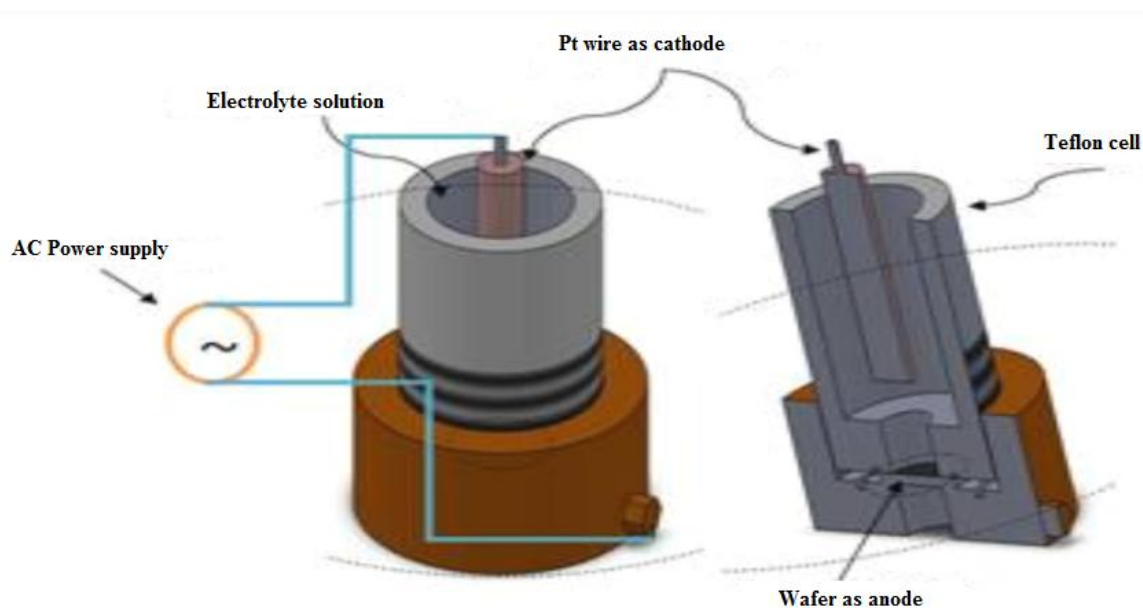


**Figure 1.** Experimental set-up of porous silicon (PS) fabrication.

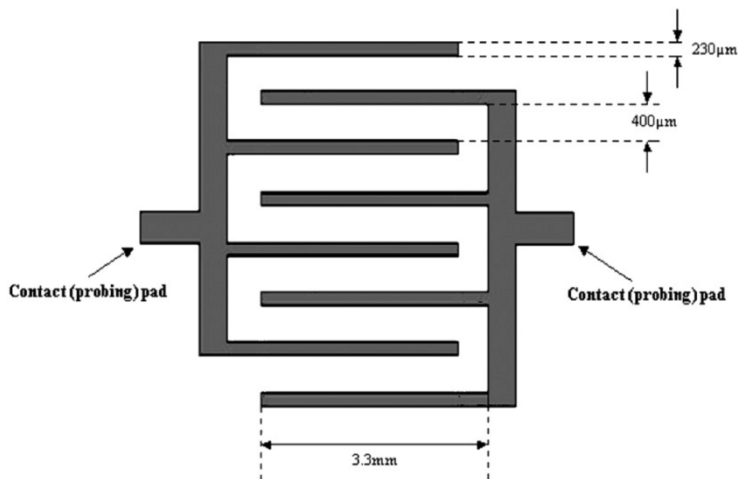


**Figure 2.** The schematic diagram of photodetector.

The formation of PS layer is using the AC process in the chemical solutions HF: ethanol (1:4) at different current density; 20, 25, 30 mA/cm<sup>2</sup> of 30 min under external incandescent light. To obtain photodetectors, metal-semiconductor-metal (MSM) contacts are fabricated by depositing silver (Ag) with thickness about 200 nm onto the PS surface. Ag is used as Schottky contact since it has the highest metal work function. The structure of MSM photodetector consists of two interdigitated

Schottky contact (electrode) with finger width of 230  $\mu\text{m}$ , finger spacing of 400  $\mu\text{m}$  and the length of each electrode is about 3.3 mm. Each electrode has four fingers as schematically shown in Fig. 2.

Contact annealing was done at 450° C for 30 min to pledge Schottky contact as well as to improve the contact properties.

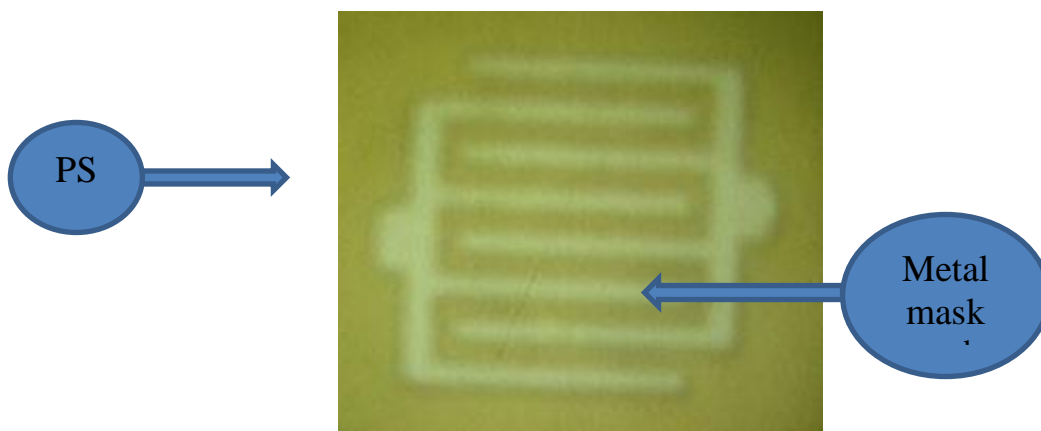


**Figure 3.** Metal mask contacts pattern of MSM photodetector.

Figure 3 shows the fabrication of contacting pad of MSM photodetector array was followed after the formation of metal mask fingers. The AC into PS was characterized by high resolution Field-Emission Scanning Electron Microscope (FE-SEM), (NOVA NANO SEM 450) and analyzed using metal finger mask that deposited by (electron beam evaporator ATO 306 vacuum coater), Keithley electrometer (model 6517A) was used to measure the current-voltage (I-V) characteristic and current-time (I-T) at room temperature. The spectral responsivity of PS-based devices was measured using a monochromator (Jabin-Yvon Co.).

### 3. RESULTS AND DISCUSSION

The frequency of AC is important to determine the PS properties and is found to be in order of 50 Hz to obtain a uniform layer. A high frequency cannot be applied since the electrochemical process has a characteristic time constant in the range of microseconds limiting the frequency of few kilohertz [3].

The effect of increasing etching current density on the morphological properties of PS layer was investigated. The FE-SEM image of Fig. 4a of PS etched at a current density of 20  $\text{mA}/\text{cm}^2$  exhibits two regions on the surface, pores with pits. The pits indicate a start of etching process on the silicon wafer. Increasing etching current density to 25  $\text{mA}/\text{cm}^2$  (Fig. 4b) causes an increase in the pore diameter and different porous morphology. The etching rate increases as a function of etching conditions, such as HF:ethanol concentration, etching duration and current density [8]. Pores are distributed regularly on the surface. A more uniform distribution of pores was obtained when the

current density was increased to  $30 \text{ mA/cm}^2$  as shown in Fig. 4c, the more homogeneous distribution of pores was obtained compared with other wafers that prepared with different electrolyte compositions [9].

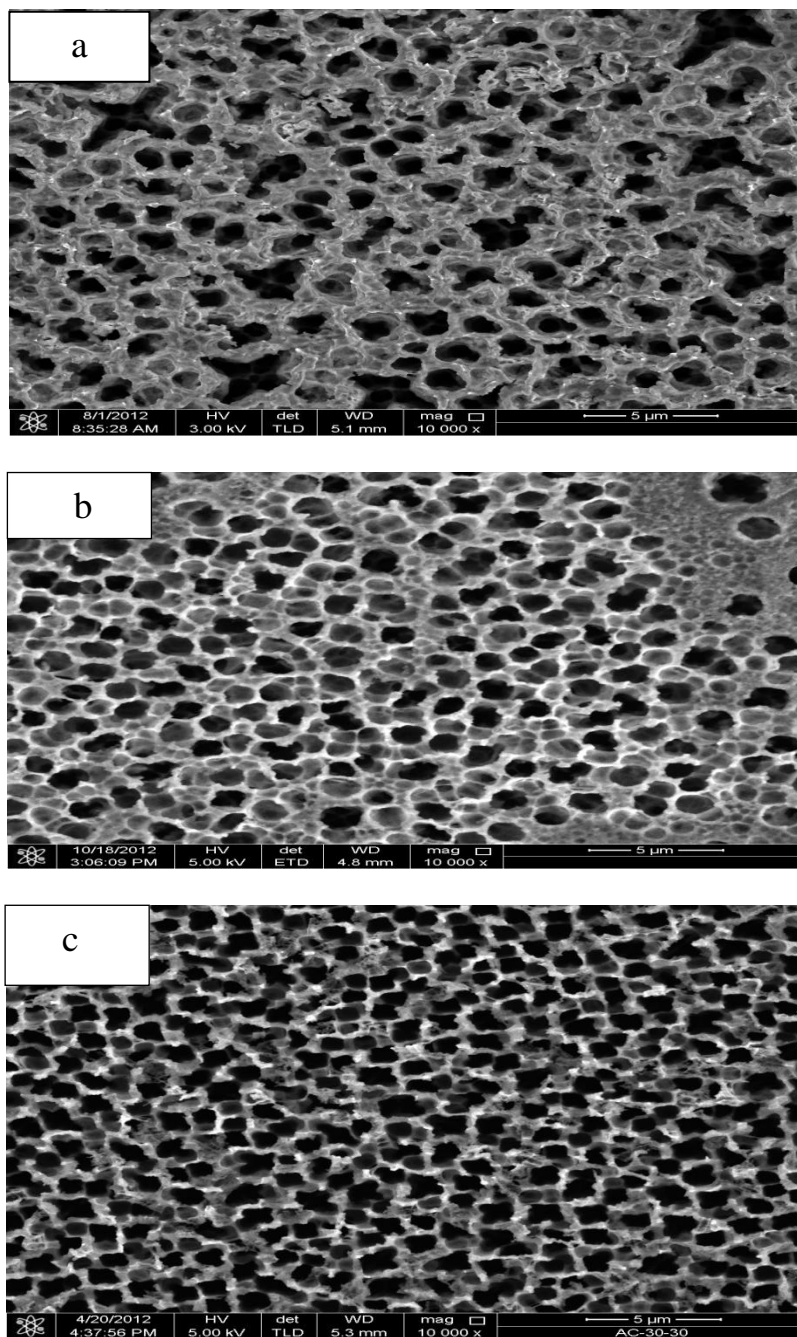


**Figure 4.** FE-SEM images of PS prepared at etching time of 30 min and different current density (a)  $20 \text{ mA/cm}^2$  (b)  $25 \text{ mA/cm}^2$  (c)  $30 \text{ mA/cm}^2$ .

This could be attributed to the presence of ethanol, active surface agent that removes hydrogen bubbles during etching and reduces surface tension [10]. FE-SEM is important to evaluate the porosity percentage using gravimetric measurements method (weight method) [11].

$$P(\%) = (m_1 - m_2) / (m_1 - m_3) \quad (1)$$

where  $m_1$  is the sample weight before etching,  $m_2$  is the sample weight after etching and  $m_3$  is the sample weight after removing the PS layer with 3% KOH or 20% NaOH solution. A summary of PS characteristic at different current densities and fixed etching time is given in Table 1. These results are explained basing on etching rate, where etching rate increases with silicon dissolution efficient accompanied with the production of PS.

**Table 1.** Etching current density and etching time correspond to porosity percentage of PS.

Etching current density (mA/cm <sup>2</sup> )	(HF:ethanol) ratio	Etching Time (min.)	Porosity (%)
20	1:4	30	32.3
25	1:4	30	45.97
30	1:4	30	53.79

This leads to formation heterojunction device between PS layer and the silicon substrate [12]. When metal makes contact with semiconductor, a barrier is formed at the metal- semiconductor interface. This barrier is responsible for controlling the current conduction as well as its capacitance behavior.

Figure 5 shows current-voltage (I-V) characteristics of PS MSM photodetector, which comprised back-to-back Schottky diode from -5 to 5V with Ag electrodes, where measured under dark and illumination (tungsten lamp) conditions as a function of different etching current densities. The variation in forward bias characterizations is controlled by PS layer resistance. This result explains the reduction of flow current in forward bias with increasing the etching current density [13]. The porosity increases as etching current density increases and hence the resistance of PS layer becomes too high. This will reduce the forward current density. When the porosity increases, the pore wall which acts as carriers trapped will increase to form a high resistive region which decreases the current passing through the PS layer [14,15]. The response of the MSM photodetector increases with the bias voltage and it saturates gradually when the voltage is beyond 2 V; the recombination current is dominant for equilibrium case the recombination process will take place. This means that each excited electron from valance to conduction band will recombine with a hole in valance bond. At high voltage region, the thermionic emission and the carrier velocity increase as the biasing voltage and the current increase exponentially with the applied voltage which exceeds the potential barrier. This voltage gives the electron enough energy to overcome the barrier height that is called diffusion current [15].

Under dark condition, the current at 5 V is found lowest than the illumination at the same bias voltage. This shows that the light illumination can effectively create electron-hole pairs in PS and greatly increases the carrier density. While, under illumination condition, light impinges onto the PS layer, the high energy photons are absorbed by PS layer to produce more electron-hole pairs, the application of a bias voltage to Ag contact creates an electric field within the underlying PS layer that

sweeps the photo-generated carriers out of the depletion region, resulting in photocurrent with voltage [16].

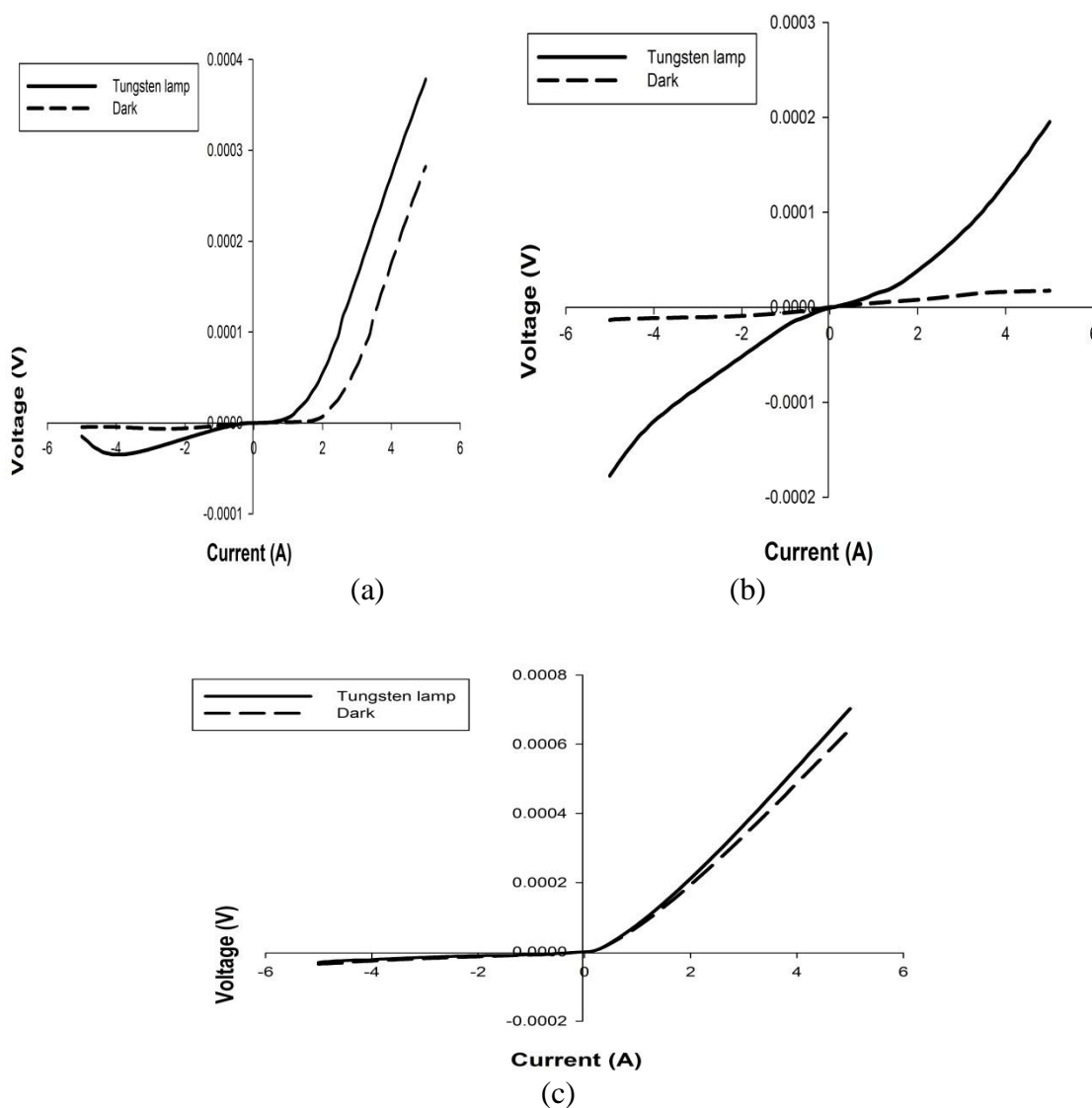


**Figure 5.** The I-V characteristics of MSM photodetector prepared under different dark and illumination conditions at (a) 20 mA/cm<sup>2</sup> (b) 25 mA/cm<sup>2</sup> (c) 30 mA/cm<sup>2</sup>.

This indicates that PS beneath the Ag MSM electrodes and plays a major role in reducing the dark current, meanwhile enhancing the photocurrent [17,18]. The Schottky barrier height (SBH) can be derived using forward- biased I-V curves. By assuming the flow current mechanism is governed by the thermionic emission conditions, the SBH can be determined from the I-V measurements based on eq. (3). Figure 6 shows a plot of lnI as a function of voltage to calculate the barrier height for Ag contact on PS at different current density, where measured under illumination and dark conditions. The  $\Phi_B$  and  $n$  were determined by using thermionic emission equation [19]:

$$I = I_0 \left[ \exp \left\{ \frac{qV}{nKT} \right\} - 1 \right] \tag{2}$$

$$I_0 = A^{**} A T^2 \exp \left\{ -\frac{q\Phi_B}{KT} \right\} \tag{3}$$

where  $I_0$  is the saturation current density based on thermionic emission theory,  $n$  is slope parameter for ideal devices equals 1,  $K$  is Boltzmann's constant,  $T$  is the absolute temperature,  $A^{**}$  is the effective Richardson coefficient,  $A$  is area of the Schottky contact is equal to  $1.5 \times 10^{-4} \text{ cm}^2$ ,  $q$  is the electron charge and  $\Phi_B$  is the barrier height. The theoretical value of  $A^*$  can be calculated using:

$$A^{**} = 4\pi m^* q K^2 / h^3 \tag{4}$$

where  $h$  is the Planck's constant and  $m^* = 0.93 m_0$  is the effective electron mass for n-Si. The value of  $A^{**}$  is determined to be  $112 \text{ Acm}^{-2}\text{K}^{-2}$  for n-Si [20]. For determining the ideality factor and Schottky barrier height of fabricated devices, a linear line was obtained by plotting the logarithm of current verses voltage from the I-V characteristics data. From eq. (3), the slop of this line is  $q/nKT$  and y- intercept is  $\ln I_0$  [21].

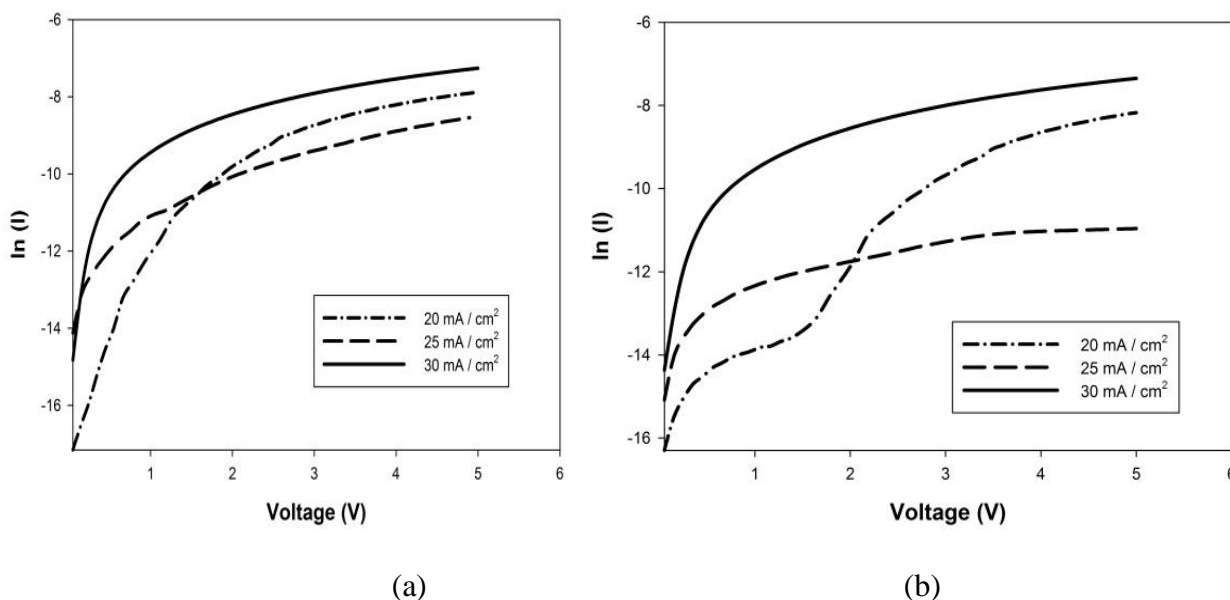


**Figure 6.** Barrier height for Ag contact on PS under (a) illumination and (b) dark conditions for different etching current densities.

Table 2 summarizes electrical measurements at 2V of SBH, ideality factor, saturation and leakage currents for 20, 25 and 30 mA/cm<sup>2</sup>.

**Table 2.** The Schottky barrier height (SBH), ideality factor (n), saturation and leakage currents under illuminated and dark conditions of PS at different etching current densities.

	20 mA/cm <sup>2</sup>		25 mA/cm <sup>2</sup>		30 mA/cm <sup>2</sup>	
	Illuminated	Dark	Illuminated	Dark	Illuminated	Dark
Current (A) at 2 V	$6.03 \times 10^{-5}$	$9.1 \times 10^{-6}$	$4.11 \times 10^{-5}$	$8.11 \times 10^{-6}$	$2.22 \times 10^{-4}$	$2.07 \times 10^{-4}$
SBH (eV)	0.53	0.55	0.54	0.56	0.56	0.59
Ideality factor (n)	6	7.5	4.06	6.7	2.2	3.7
Saturation current (A)	$1.96 \times 10^{-6}$	$9.05 \times 10^{-7}$	$1.33 \times 10^{-6}$	$6.1 \times 10^{-7}$	$6.15 \times 10^{-7}$	$1.93 \times 10^{-7}$

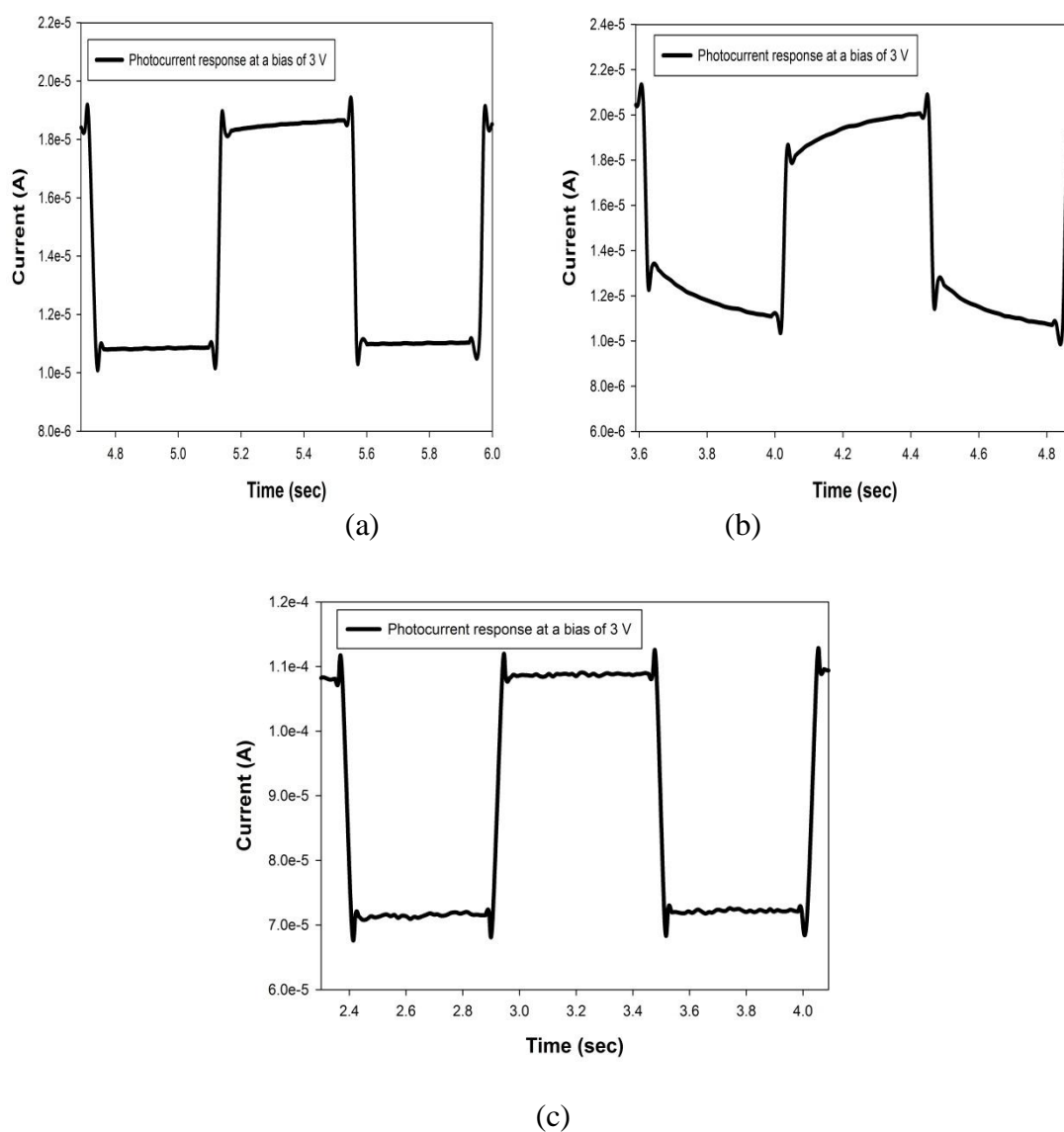


**Figure 7.** The photoresponse of the photoconductor device for repetitive switching of the blue illumination at V=3 V applied across two electrodes for (a) 20 mA/cm<sup>2</sup> (b) 25 mA/cm<sup>2</sup> (c) 30 mA/cm<sup>2</sup>.

Figure 6 indicates that it gets smaller values under illumination than under dark condition. However, it can be seen that the difference of SBH between illumination and dark conditions for 20, 25 and 30 mA/cm<sup>2</sup> is 0.02, 0.02 and 0.03 eV, respectively. This indicates that 30 mA/cm<sup>2</sup> has higher change in SBH. Moreover, it should be noted that the low dark current in 30 mA/cm<sup>2</sup> could be due to the enhancement of SBH, which reveals that 30 mA/cm<sup>2</sup> is more sensitive to illumination. The surface roughening also plays an important role on the interface between the metal, PS surface and resulting in improvement of the electrical properties [22]. Furthermore, the values of ideality factor are quite near to unity which indicated good quality of Schottky contacts and thin interface layer. Thin layer may be responsible for the lower dark current [23]. The high etching current density (high porosity) may move the surface Fermi level downward to the valence band and thus increase the SBH to result in a reduction in the leakage current [21].

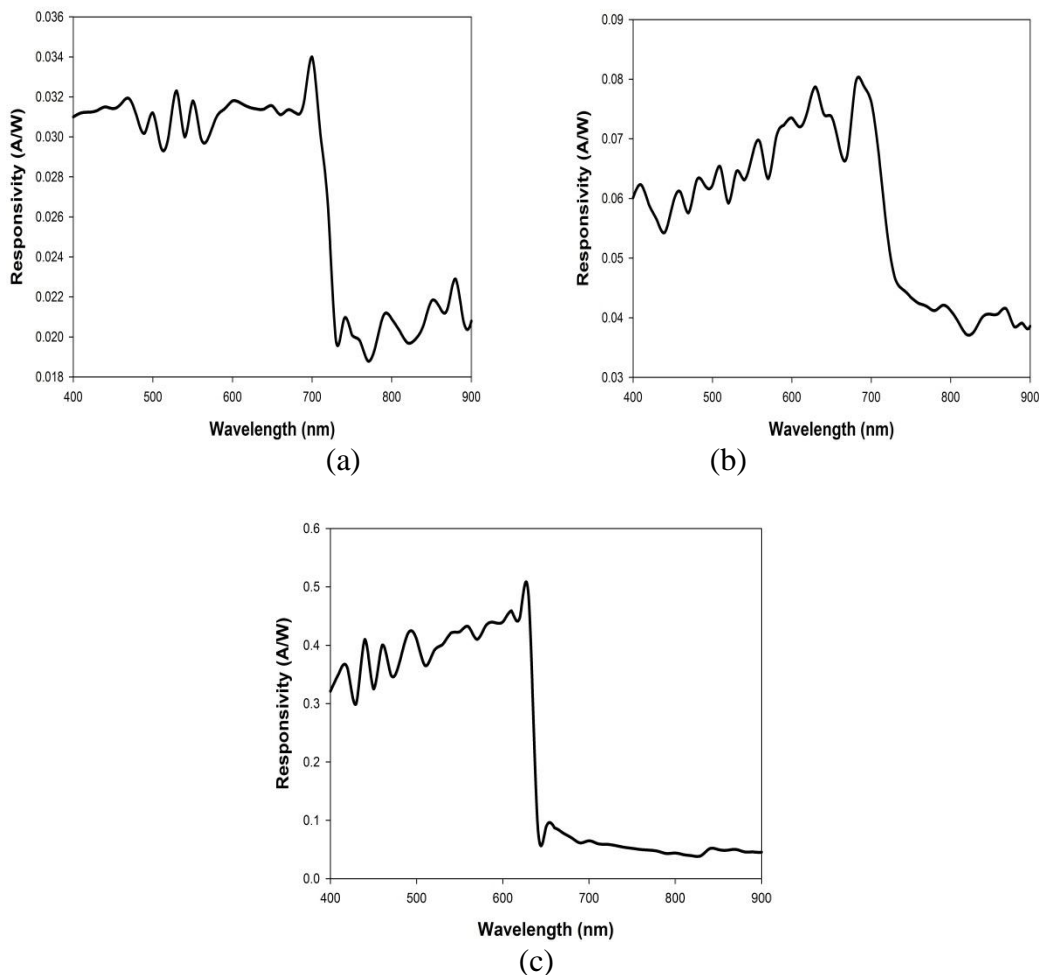
The photoresponse (on-off response) of the device measured for repetitive switching of the blue light illumination ( $\lambda=460$ , intensity  $I=70000$ ) with a constant voltage of 3 V applied across the two electrodes is shown in Fig. 7. The rise time of photoconductive device was obtained under different current densities 20, 25 and 30 mA/cm<sup>2</sup> to be 0.0279 s, 0.0114 s and 0.029 s, respectively corresponds to the decay time that was obtained to be 0.0281 s, 0.0127 s and 0.023 s. One can also see from Fig. 7, the intensity of the blue illumination increases as the etching current density increases. In case of high current density (high porosity), the good response times are mainly attributed to the lack of defects in PS. The fast response in MSM photodetector is usually related to the transit time of photo-generated carriers [24], while the slow response in a PS MSM photodetector is usually attributed to the oxygen adsorption at the surface and grain boundaries [25,26].

Figure 8 shows the measured spectral responsivity  $R$  (A/W) as a function of wavelength for MSM photodetector. Photodetector responsivity was measured as a function of the incident light wavelength through xenon lamp. The measurements were achieved in the range of 400-900 nm under 5 V applied bias, it shows that the spectral responsivity lies within the visible region, while the peak and value of spectral responsivity are varied for different etching current densities. The light responsivity ( $R$ ) of PS was calculated using the following relationship [27]:

$$R = \frac{I_{ph}}{P_{inc}} \quad (5)$$

where  $I_{ph}$  is the photocurrent which represents the number of incident photons and  $P_{inc}$  is the incident optical power. The light wavelengths of the fabricated Ag PS MSM photodetector was obtained for different current densities 20, 25 and 30 mA/cm<sup>2</sup> of about 699.32 nm, 683.43 nm and 626.37 nm and the maximum peak responsivities were obtained to be 0.0339 A/W, 0.08 A/W and 0.5 A/W, respectively. The variation of the spectral responsivity depends mainly on the thickness of the photoactive layer and the electrode coverage [28], the high response corresponds to the thicker layer, normally high porosity (resulted from 30 mA/cm<sup>2</sup>) produce thick layers. This can be explained in terms of porosity increasing. Indeed, the increasing of porosity leads to increasing the electron-hole pair in the depleted region as a consequence of a decrease of absorbed photons by PS and strong absorption by silicon [29]. This is a logical result because a high thickness of PS has to produce more

electron–hole pair; however, the photodetector of etching current density  $30 \text{ mA/cm}^2$  produces a larger responsivity. It seems the recombination process takes importance because of the larger way of the pair generated to arrive at external contact [30]. Finally, it can be seen that almost all the spectral responses of photodetectors have a maximum value around 600 to 700 nm.



**Figure 8.** The responsivity of Ag/PS/Ag as the function of the wavelength for MSM photodetectors prepared for (a)  $20 \text{ mA/cm}^2$  (b)  $25 \text{ mA/cm}^2$  (c)  $30 \text{ mA/cm}^2$ .

Quantum efficiency ( $\eta$ ) is an important parameter to evaluate the performance of photosensitive device; it is related to the number of electron-hole pairs excited by absorbed photons and is given by [31]:

$$\eta = R \times \frac{hc}{q\lambda} \tag{6}$$

where  $\eta$  is the quantum efficiency,  $\lambda$  is the incident light wavelength,  $h$  is Planck constant and  $c$  is the speed of light. From eq. (6), the quantum efficiency was obtained under different current densities 20, 25 and  $30 \text{ mA/cm}^2$  to be 6.01%, 14.5% and 99.5%, respectively. This high quantum

efficiency may be attributed to the high internal gain. According to Liu et al. [32], this indicated that a Schottky barrier at the metal electrode semiconductor interface can exhibit hole-trapping in the reversed-bias junction that shrinks the depletion region and allows tunneling of additional electrons into the photoconductor; if electrons pass multiple times, this mechanism yields photoconductive gain greater than unity. Moreover, their evolution as a function of etching current density is also identical to those of spectral responsivity. Thus, the interpretation of these spectra and their evolution as a function of etching current density is the same to those of spectral responsivity.

#### 4. CONCLUSION

The AC within ECE gave successful results for forming PS. The SEM results exhibit at 30 mA/cm<sup>2</sup> high porosity and uniformed distribution at 30 min. It is found that under illumination condition, the current and ideality factor have inversely correlation with current density, while saturation and leakage currents correlate directly with current density. The effect of current density is observed on photoresponse and responsivity. The results gave distinguished quantum efficiency of photodetectors performance of 30 mA/cm<sup>2</sup>.

#### ACKNOWLEDGEMENTS

This work has been achieved using FRGS Grant No.: 9003-00249. One of us (Y.A.) would like to acknowledge the TWAS – Italy, for the fully support of his visit to JUST – Jordan under TWAS-UNESCO Associateship.

#### References

1. T. Hadjersi, N. Gabouze, *Optical Mater.*, 30 (2008) 865.
2. L. Canham, *Properties of Porous Silicon*, EMIS, Data Reviews Series, 18, London (UK) pp.199
3. A. El-Bahar, Y. Nemirovsky, *Appl. Phys. Lett.*, 77 (2000) 208.
4. A. V. Brodovoi, V. A. Brodovoi, V. A. Skryshevskiy, S. G. Bunchuk, L. M. Khnorozok, *Semicond. Phys. Quan. Electro. Optoelectro.*, 5 (2002) 395.
5. N. Naderi, M. R. Hashim, *Appl. Sur. Sci.*, 258 (2012) 6436.
6. Y. Al-Douri, N.M. Ahmed, N. Bouarissa, A. Bouhemadou, *Materials and Design*, 32 (2011) 4088.
7. S. Basu, J. Kanungo, *Nanocrystalline porous silicon*, in: S.Basu (Ed.), *Crystalline silicon–properties and uses*, In Tech. Croatia (2011)
8. C. Gamato, Delerue, H. J. Bardeleben, *Structural and Optical Properties of Porous Silicon Nanostructures*, in Y. Kanemitsu (Ed.), *Silicon-based nanostructures*, CRC Press, USA (1998)
9. T. H. Gfroerer, *Photoluminescence in Analysis of Surfaces and Interfaces*, in: R.A. Meyers (Ed.), *Encyclopedia of analytical chemistry*, John Wiley & Sons Ltd, Chichester (2000)
10. J. Erlebacher, K. Sieradzki, P. C. Searson, *J. Appl. Phys.*, 76 (1994) 182.
11. V. Lehmann, U. Gösele, *Appl. Phys.*, 58 (1991) 856.
12. A. M. Rosi, H. G. Bohn, *phys. Stat. solidi (a)*, 202 (2005) 1644.
13. A. A. J. Hussain, A. M. Alwan, N. M. Ahmed, *Investigations of Porous Silicon Photodetector*, LAP Lambert Academic Publishing, Germany (2011)

14. L. A. Balagurov, D. G. Yarkin, G. A. Petrovicheva, E. A. Petrova, A. F. Orlov, S. Ya. Andryushin, *J. Appl. Phys.*, 82 (1997) 4647.
15. G. Algun, M. G. Arikan, *J. Phys.*, 23 (1999) 789.
16. A. F. Abd Rahim, M. R. Hashim, N. K. Ali, *Physica B*, 406 (2011) 1034.
17. M.K. Lee, Y.H. Wang, C.H. Chu, *IEEE J. Quan. Electro.*, 33 (1997) 2199.
18. M. K. Lee, Y.C. Tseng, C. H. Chu, *Appl. Phys. A*, 67 (1998) 541.
19. E.H. Rhoderick, R.H. William, *Metal–Semiconductor Contacts*, 2<sup>nd</sup> edition, Oxford University Press, New York (1998)
20. V. Bougrov, M. Levinshstein, S. Rumyantsev, A. Zubrilov, *Gallium Nitride (GaN)*, in: M. E. Levinshstein (Ed.), *Properties of Advanced Semiconductor Materials: GaN, AlN, InN, BN, SiC, SiGe*, John Wiley & Sons, Inc. NY-Chichester-Weinheim-Brisbane-Singapore-Toronto (2001)
21. J.M. Perez, J. Villalobos, P. McNeill, J. Prasad, R. Cheek, J. Kelber, J.P. Estrera, P.D. Stevens, R. Glosser, *Appl. Phys. Lett.*, 61 (1992) 563.
22. Y.C. Lee, Z. Hassan, M.J. Abdullah, M.R. Hashim, K. Ibrahim, *Microelectro. Eng.*, 81 (2005) 262.
23. L. S. Chuah, Z. Hassan, N. Shamsuddin, N. Amirruddn, C. W. Chin, H. A. Hassan, *Optoelectro. Adv. Mater.-Rapid Commun.*, 2 (2008) 650.
24. H.I. Abdulgafour, Z. Hassan, F.K. Yam, K. AL-Heuseen, Y. Yusof, *Appl. Sur. Sci.*, 258 (2011) 461.
25. Y. Takahashi, M. Kanamori, A. Kondoh, H. Minoura, Y. Ohya, *Jap. J. Appl. Phys.*, 33 (1994) 6611.
26. D.H. Zhang, *J. Phys. D: Appl. Phys.*, 28 (1995) 1273.
27. S. S. Islam, *Semiconductor physics and device*, Oxford University press, Delhi (2004)
28. K. Honkanen, *Fabrication and modelling of SOI and GaAs MSM photodetector and a GaAs- based integrated photoreceiver*, Ph.D thesis, Helsinki University of Technology, Finland (2001)
29. T. Hadjersi, N. Gabouze, *Optical Mater.*, 30 (2008) 865.
30. G. G. Salgado, R. Hernandez, J. Martinez, T. Diaz, H. Juarez, E. Rosendo, R. Galeazzi, A. Garcia, G. Juarez, *Microelectro. J.*, 39 (2008) 489.
31. L. Li, P. Wu, X. Fang, T. Zhai, L. Dai, M. Liao, Y. Koide, H.Q. Wang, Y. Bando, D. Golberg, *Adv. Mater.*, 22 (2010) 3161.
32. K.W. Liu, J.G. Ma, J.Y. Zhang, Y.M. Lu, D.Y. Jiang, B.H. Li, D.X. Zhao, Z.Z. Zhang, B. Yao, D.Z. Shen, *Solid-State Electro.*, 51 (2007) 757.